


## Article

# Study of a Gas Turbine Cycle to Boost the Autonomy of Electric Cars

Joelle Najib \*, Maroun Nemer and Chakib Bouallou 

Centre for Energy Efficiency (CES), Mines ParisTech, PSL Research University, 60 Bd St Michel, F-75006 Paris, France; maroun.nemer@mines-paristech.fr (M.N.); chakib.bouallou@mines-paristech.fr (C.B.)

\* Correspondence: joelle.najib@mines-paristech.fr

**Abstract:** The greenhouse gas emissions from the transportation sector are the primary cause of climate change. As a result, many studies have developed new powertrains with reduced CO<sub>2</sub> emissions for the automotive industry. The gas turbine cycle coupled to an alternator is an autonomy booster for series hybrid electric vehicles. Many gas turbine configurations are proposed in the literature to obtain the highest cycle efficiency. This paper suggests a new architecture offering higher efficiency than all the previous cycles. The two-step methodology consists at first of a sensibility analysis using VBA and Refprop to determine the optimal operating conditions in terms of higher efficiency. The selected cycle consists of two compression stages with an intercooler, a combustion chamber, a cooled hot pressure turbine, an uncooled low-pressure turbine, and a recuperator. The efficiency of this design reaches 51.39%, which approximately matches the designs compared in the literature, but is more compact because it does not require a second combustion chamber.

**Keywords:** turbine cooling; convection cooling; gas turbine; range extender; series hybrid electric vehicles



**Citation:** Najib, J.; Nemer, M.; Bouallou, C. Study of a Gas Turbine Cycle to Boost the Autonomy of Electric Cars. *Energies* **2022**, *15*, 3348. <https://doi.org/10.3390/en15093348>

Academic Editors: Petar Varbanov, Xuexiu Jia and Xue-Chao Wang

Received: 24 February 2022

Accepted: 2 May 2022

Published: 4 May 2022

**Publisher's Note:** MDPI stays neutral with regard to jurisdictional claims in published maps and institutional affiliations.



**Copyright:** © 2022 by the authors. Licensee MDPI, Basel, Switzerland. This article is an open access article distributed under the terms and conditions of the Creative Commons Attribution (CC BY) license (<https://creativecommons.org/licenses/by/4.0/>).

## 1. Introduction

The road transportation sector emitted around 70% of the greenhouse gas emissions from the transport sector in 2014 [1]. Therefore, moving towards zero-emission vehicles is a top priority. Among different powertrains, gas turbines (GTs) have attracted the interest of automotive manufacturers due to their numerous advantages in vehicular applications. The major benefit of gas turbines is their ability to operate on a variety of fuels. Gas turbines are compact and reliable engines with a reduced number of moving parts, reduced vibration, and low exhaust emissions in comparison with internal combustion engines [2]. The study conducted by Christodoulou et al. [3] shows that the micro-gas hybrid vehicle offers a fuel consumption reduction of 23% for heavy vehicles. In addition, the noise emissions of the GTs are about 5 dB less than those of diesel engines.

In discussing this topic, it is important to investigate the history of GTs in vehicles as prime movers and then, as range extenders. In addition, an overview of the simplest configuration of the GT cycle and its main components is presented.

In 1954, Chrysler Corporation presented several gas turbine (GT) cars introducing a revolutionary feature: the heat exchanger [4]. Then, they revealed seven generations of GT cars with different improvements on various components. As Chrysler produced 50 turbine cars, Volkswagen signed a contract with Williams Research Corporation and developed the microbus station wagon [5]. Additional prototypes for heavy vehicles were also produced such as the 1965 Chevrolet Turbo Titan III propelled by a GT-309 engine operating at 35,000 rev/min and the 1972 GMC Astro Gas Turbine [6]. There have been prototypes of other GT cars in racing vehicles such as the Rover-BRM that participated in Le Mans in 1963, Formula 1 in 1971, and the Lotus 56 [7]. However, their high fuel consumption and slow acceleration restrict their application in the marketplace. These

problems result from operating the GT systems at high speed even at idle conditions, and mechanically coupling the turbine to the vehicle-driving load.

Recent studies have focused on using GTs as auxiliary power units as a solution to the limited range and high cost of electric cars. The GTs are combined with a generator, so the mechanical work of the turbine is converted to electric power [8]. Figure 1 illustrates the proposed configuration. This configuration is a solution for both the environmental emissions and the limited autonomy range of electric cars. Its main advantage compared with the previous configurations is that the GT cycle operates independently from the vehicle speed. Hence, the optimal operating point of the GT is easily controllable to obtain the GT's highest efficiency.

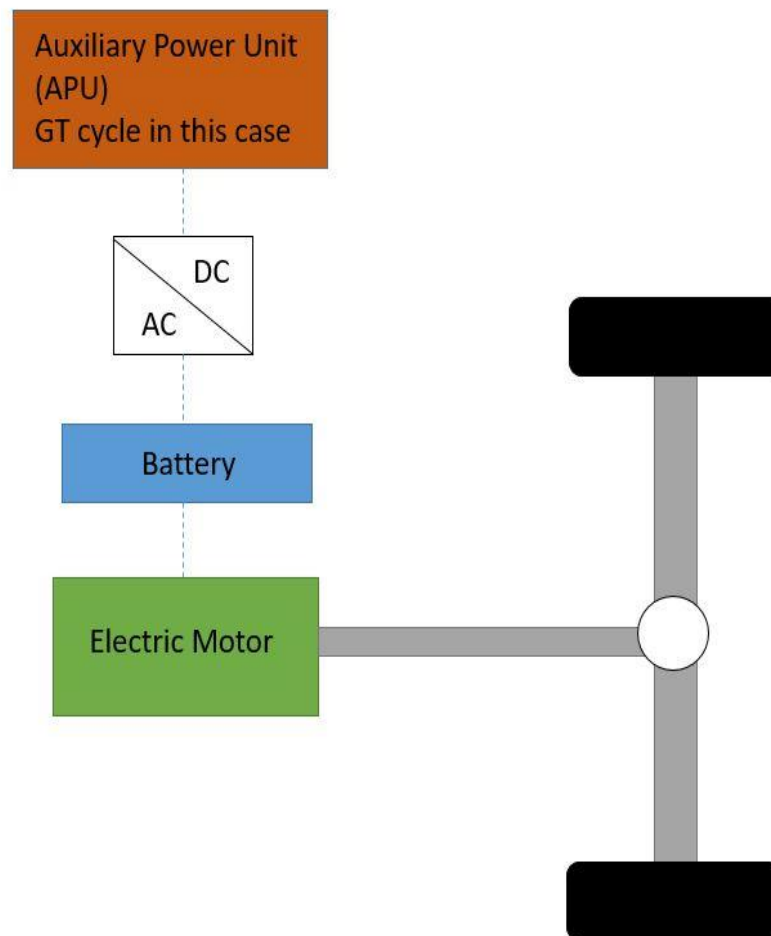


**Figure 1.** Gas turbine as an auxiliary power system for series hybrid electric vehicles.

Some automobile manufacturers have developed series hybrid electric vehicles (SHEV) using GTs as autonomy extenders. Table 1 summarizes the different configurations of series hybrid electric vehicles with their properties extracted from [9].

In its simplest form, the GT operates according to the Brayton cycle. It is composed of a centrifugal compressor, a combustion chamber, and a radial turbine. The mechanical drive is divided into three main categories. The first category is illustrated in Figure 2. It consists of the compressor and the turbine mounted on the same shaft and the alternator either on the compressor side or on the turbine side. In this case, the output shaft has the same speed as the turbine/compressor shaft and is used to drive electric generators coupled or not with the gearbox. This configuration is convenient when the gas turbine is required to operate at a constant speed [10].

**Table 1.** State-of-the-art of SHEV configurations of different automotive manufacturers.

Automotive Manufacturers	SHEV Properties
General Motors	40 kW turbine in EV-1 series
Volvo	Environmental Concept Car (ECC) using recycled materials
ETV Motors	Toyota Prius equipped with a microturbine
Capstone	CTM-380 at the LA Auto show
Jaguar	Jaguar C-X75 driven by a twin-shaft turbine from Bladon Jets
Pininfarina	Range extender equipped with a diesel GT
Delta Motorsport	Microturbine incorporated into the E4 coupé
Techrules	30 kW turbine rotating at 96,000 rpm as a booster to the EV
Wrightspeed	Fulcrum GT, an intercooled recuperated GT cycle rotating at 100,000 rpm
Walmart	WAVE range extending series hybrid

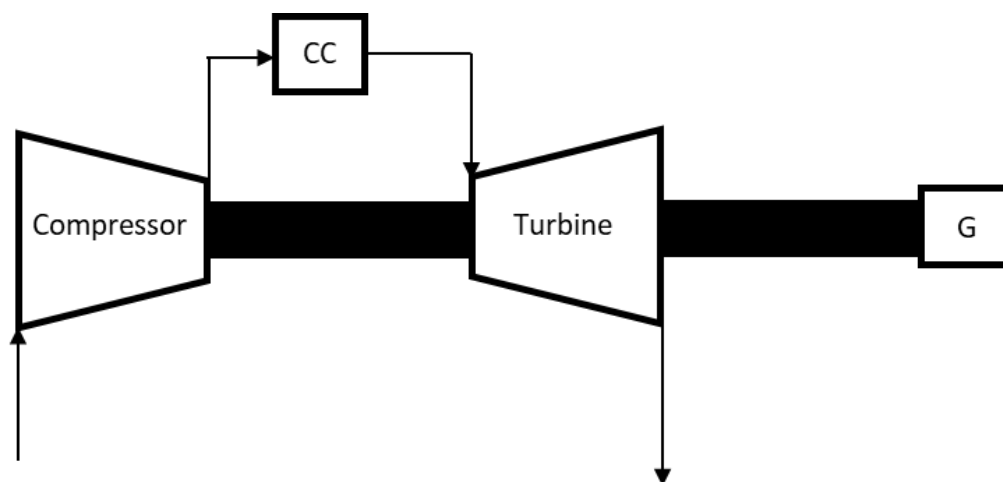


**Figure 2.** Single shaft GT cycle.

In the case of a twin-shaft turbine, a gas turbine drives only the compressor and another turbine named “the free turbine” is connected to the driven system. Figure 3 represents the twin-shaft turbine architecture. The two turbines are not coupled mechanically but aerodynamically. Thus, the compressor is driven at a steady speed and is not affected by the load [11]. The main benefit of this configuration towards the single shaft gas turbine is its flexibility and the ability to run at variable speeds.

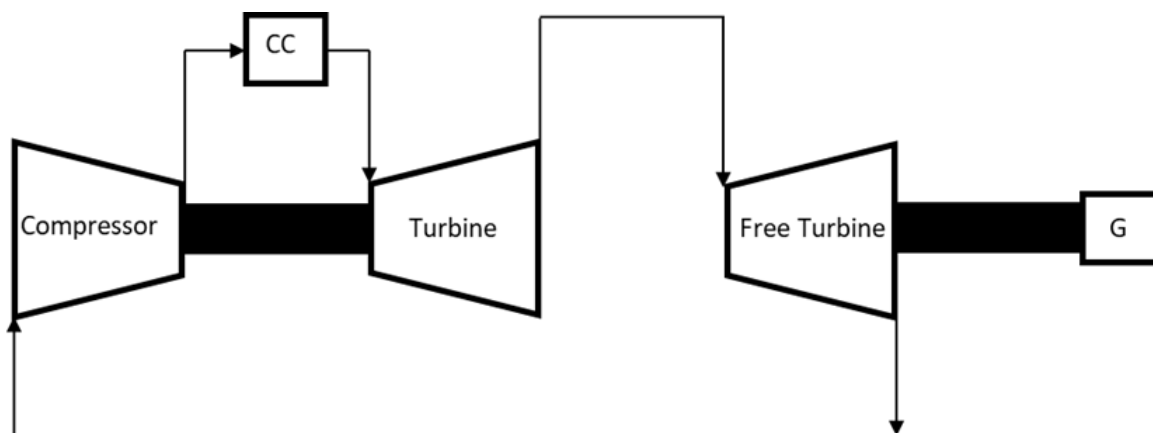


**Figure 3.** Twin-shaft GT cycle.

Another configuration is the multi-spool arrangement illustrated in Figure 4, a mechanical separation of the compressor stages. Each compressor is driven by its turbine at different rotating speeds [12]. In other words, the HP compressor is driven by the HP

turbine, and the LP compressor is driven by the LP turbine. This arrangement is generally used in high power systems.

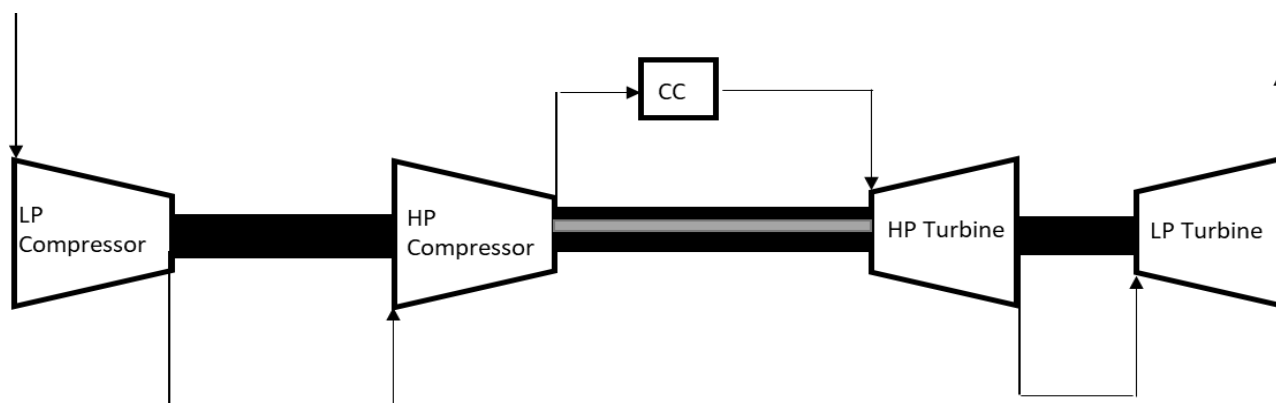


**Figure 4.** Multi-spool arrangement GT cycle.

The efficiency of the GT cycle depends on different parameters such as its architecture, its maximum pressure, and the turbine inlet temperature (TIT). The latter is related to the turbine material melting temperatures. Therefore, the turbine cooling technique is applied to increase the TIT. There are two main types of cooling: external and internal cooling. Table 2 shows a list of the various internal cooling techniques, their applications, and specifications.

**Table 2.** Internal cooling techniques, applications, and specifications.

Internal Cooling Techniques	Applications and Specifications	Reference
Convection cooling	Simple smooth cooling channel	[13]
Impingement cooling	Leading edge and mid-chord	[14]
	Plenum feeding several nozzles	
Pin fin cooling	Trailing edge	[15]
	Adding pins to the cooling channel	
Dimple cooling	Trailing edge	[16]
	Replacing pins with dimples	
Rib turbulated cooling	Adding rib turbulators	[16]
	High heat transfer coefficient	
	Complex and expensive	

After explaining the main architecture of a GT cycle, in the coming section, an overview of the most relevant studies in the literature investigating different configurations of the GT cycle as a booster for electric vehicles is presented. This study aims to propose a new GT cycle with improved efficiency and determine its optimal operating conditions. Based on the surveyed studies, a large sample of the most relevant designs was chosen to identify the selected architecture, the operating conditions as well as the efficiency, as shown in Table 3 and illustrated in Figures 5 and 6; Figure 6 is a continuation for Figure 5.

Some studies have investigated the recuperated GT cycle as extenders in electric cars. It consists of a Brayton cycle with a recuperator to recover the heat at the outlet of the turbine. Mackay [17] developed a GT cycle to drive hybrid vehicles suitable for passenger cars and small buses. The operating pressure ratio was 3 and the TIT was 816 °C. The efficiency of the current GT cycle is 30%. Ji et al. [2] conducted a numerical and an experimental study of the recuperated GT cycle. The results show that the cycle efficiency was 35% with a recuperator effectiveness of 0.7, a pressure ratio of 3.2, and a turbine inlet temperature (TIT) of 1152 K.

**Table 3.** Summary overview of the literature for GT configurations as range extenders for electric vehicles.

GT Configurations	Efficiency (%)	Conditions	Author	Figure
Recuperated GT cycle	30	Pressure ratio 3, TIT = 816 °C	Mackay [17]	Figure 5a
Recuperated GT cycle	35	Pressure ratio 3.2, TIT = 1152 K	Ji. et al. [2]	Figure 5a
Downstream-intercooled reheat external combustion GT cycle	40.7	Pressure ratio of 4, TIT = 1250 °C	Bou Nader et al. [18]	Figure 5b
Reheat GT coupled to a turbine Reheat Steam Rankine cycle	47.2	Compression ratio 3.5, Expansion ratio 4, TIT = 1250 °C	Barakat et al. [19]	Figure 5c
IRReGT cycle	47	Compression ratio 4, Expansion ratio 3.5, TIT = 1250 °C	Bou Nader [9]	Figure 6d
Intercooled Recuperated Reheated GT cycle with a cooled HP turbine	51.6	Pressure ratio 3, TIT1 = 1450 °C, TIT2 = 1100 °C	Najib et al. [20]	Figure 6e

Other researchers tackled different GT configurations. Bou Nader et al. [18] conducted an exergo-technological analysis to determine the most convenient cycle for electric cars. The identified GT cycles were prioritized based on their efficiency and net specific work. The study shows that a downstream-intercooled reheat external combustion GT cycle is the optimal realistic cycle with the highest efficiency (40.7%) for regenerator effectiveness of 0.85, a maximum pressure ratio of 4, and a TIT of 1250 °C. In contrast, Barakat et al. [19] investigated the feasibility of combined GT cycle configurations as substitutes for ICE. The cycle configuration consisted of a Brayton cycle coupled to a Steam Rankine cycle. The study was based on thermodynamic exergy, energy, and integration assessment. The reheat GT coupled to a turbine reheat Steam Rankine cycle was selected and had a system efficiency of 47.2% at a TIT of 1250 °C. In addition, Bou Nader [9] selected the Intercooled Recuperated Reheated (IRReGT) cycle as the most suitable in terms of efficiency and power density. The cycle consisted of two compression stages with an intercooler, a recuperator, and two expansion stages with reheating using two combustion chambers. The cycle efficiency was 39% for TIT = 950 °C, 43.7% for TIT = 1100 °C, and 47% for TIT = 1250 °C. The maximum compression ratio was 4 and the maximum expansion ratio was 3.5.

Inspired by [9], Najib et al. [20] suggest a new configuration of the GT cycle. By increasing the TIT, an increase in the cycle efficiency was achieved. However, it is limited by the turbine materials melting temperatures. Hence, the proposed configuration consists of an IRReGT cycle with blade cooling for the hot pressure (HP) turbine. The thermodynamic analysis showed that temperatures of 1450 °C can be reached with an increase in the cycle efficiency of 4.78 points (51.6%) compared with the basic IRReGT cycle (46.9%) for melting material temperatures of 1100 °C.

Based on the previous findings, this study develops a comprehensive methodology to propose a new efficient cycle to boost the autonomy of EVs. The suggested configuration is based on the cycle proposed by [20] because its efficiency is the highest among the presented architectures. The purpose of the study is to improve the efficiency of the current cycle by increasing the TIT at the HP cooled turbine and removing the second chamber. This paper is divided into two main parts. The first part consists of a comprehensive sensibility analysis of the recuperated gas turbine cycle to determine the optimal operating conditions such as the number of compressors and the turbine stages, the optimal pressure, and temperature. The second part discusses different scenarios of the GT HP cooling technique. The obtained results are compared with the configuration suggested by [20].

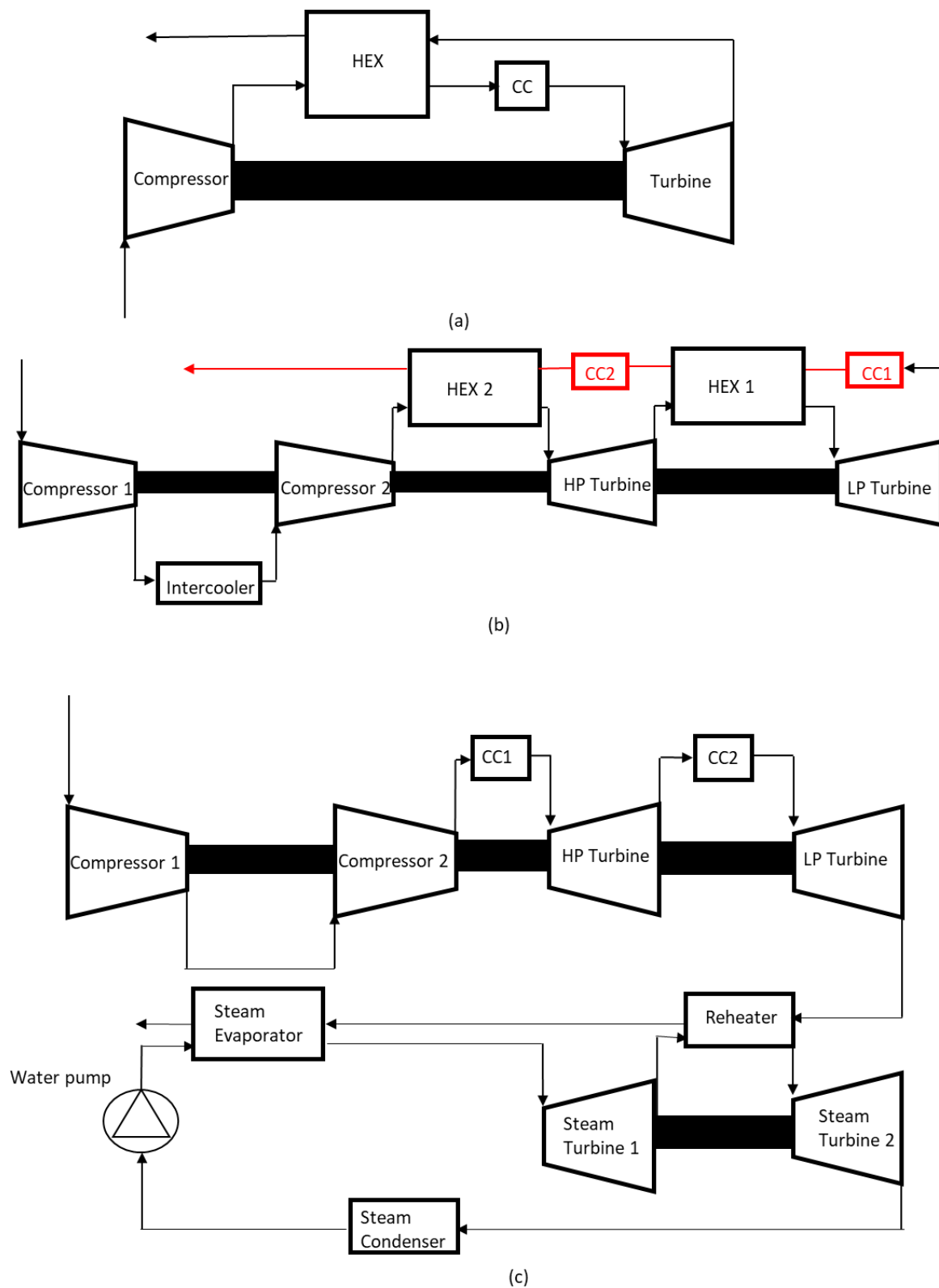


**Figure 5.** GT configurations from the literature: (a) Recuperated GT cycle, (b) Downstream-intercooled reheat external combustion GT cycle, (c) Reheat GT coupled to a turbine Reheat Steam Rankine cycle.

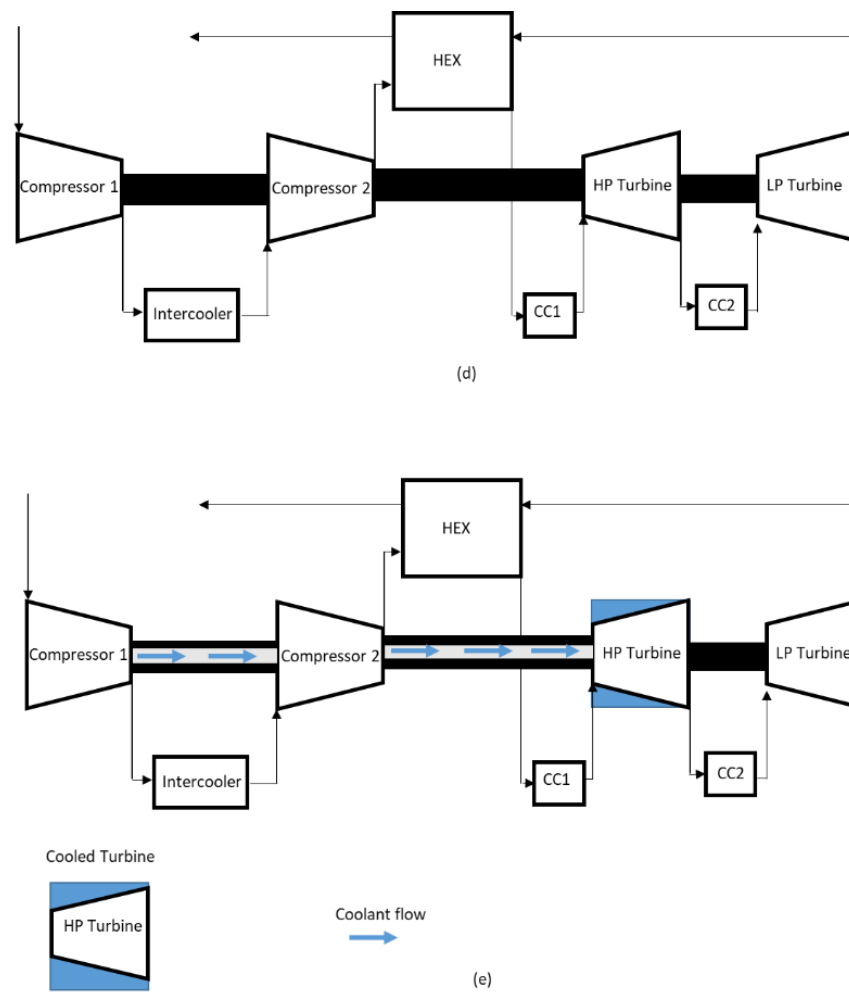


**Figure 6.** GT configurations from literature: (d) IRReGT cycle, (e) Intercooled Recuperated Reheated GT cycle with a cooled HP turbine.

## 2. Materials and Methods

### 2.1. Uncooled Cycle

This section presents the methodology applied to identify the most suitable gas turbine cycle in terms of efficiency and net specific work. The study includes an analysis to determine the optimal operating conditions at different stages of the cycle.

The thermodynamic analysis is developed using Visual Basic for Applications (VBA) and NIST REFPROP (National Institute of Standards and Technology (NIST), Colorado, USA.). The considered cycle is the recuperated gas turbine cycle represented in Figure 7. The first law of thermodynamics is applied to calculate the compressor and the turbine work, neglecting the heat transfer with the surroundings and the variation of kinetic and potential energy at the inlet and outlet of each component. The isentropic efficiency of the compressor, the turbine, and the recuperator are considered constant and equal to 0.8, 0.85, and 0.8, respectively, based on Chrysler gas turbine vehicles [4] and Bou Nader [9]. TIT is limited by the material melting temperatures. When using low-cost materials the TIT is limited to 950 °C [21]. The thermodynamic analysis takes into consideration the air/fuel ratio in the combustion chamber. The reaction is a lean mixture combustion between air and the fuel, the latter is the methane. When compressor stages are increased, an intercooler is added to cool the compressed air before it enters the next compressor stage. The intercooler is subjected to ambient conditions, and due to pinch, the temperature at its outlet is assumed to be 35 °C.

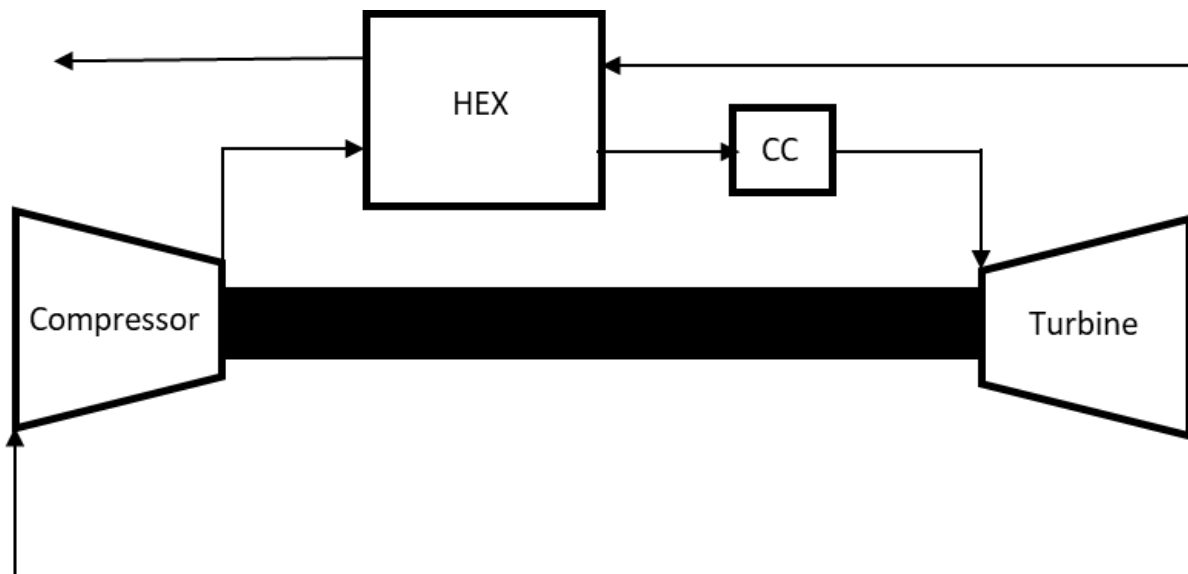
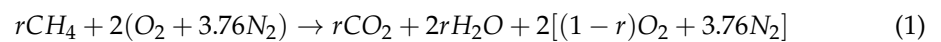


Figure 7. Recuperated gas turbine cycle.

The combustion of the methane is presented in Equation (1):

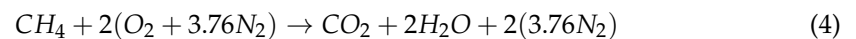


$$\lambda = \frac{1}{r} \quad (2)$$

$r$  is the ratio between the real fraction of fuel mass flow ( $m_c$ ) to air mass flow ( $m_a$ ) to the stoichiometric fraction calculated as shown in Equation (3):

$$r = \frac{\left(\frac{m_f}{m_a}\right)_{real}}{\left(\frac{m_f}{m_a}\right)_{st}} \quad (3)$$

$\left(\frac{m_f}{m_a}\right)_{st}$  is calculated from the stoichiometric equation of the methane combustion presented below:



$$\left(\frac{m_f}{m_a}\right)_{st} = \left(\frac{m_f}{m_{O_2}}\right) \times \left(\frac{m_{O_2}}{m_a}\right) = \left(\frac{16}{64}\right) \times 0.23 = 0.0575 \quad (5)$$

After the first combustion chamber, the remaining mass of the different components at the exit of the combustion chamber are calculated using Equations (6)–(10):

$$Y_{CH_4} = 0 \quad (6)$$

$$Y_{O_2} = \frac{2 \times (1-r) \times 32}{m_t} \quad (7)$$

$$Y_{N_2} = \frac{7.52 \times 28}{m_t} \quad (8)$$

$$Y_{CO_2} = \frac{44 \times r}{m_t} \quad (9)$$

$$Y_{H_2O} = \frac{2 \times 18 \times r}{m_t} \quad (10)$$



The total mass ( $m_t$ ) is obtained using Equation (11):

$$m_t = 16r + 2 (32 + 2.76 \times 28) = 16r + 274.56 \quad (11)$$

In order to check if combustion can occur in a new combustion chamber, the remaining oxygen mass should be verified and should not be zero. Then, the products of the previous combustion equation are taken as reactants and Lavoisier's law of conservation of mass is applied. The same methodology is used to determine the components at the exit of each additional combustion chamber.

The compressor work is obtained by Equation (12):

$$W_C = h_{C-outlet} - h_{C-inlet} \quad (12)$$

$W_C$ : Compressor specific work (J/kg)

$h_{C-outlet}$ : Specific enthalpy at compressor outlet (J/kg)

$h_{C-inlet}$ : Specific enthalpy at compressor inlet (J/kg)

The expression used for the turbine is presented in Equation (13):

$$W_T = h_{T-inlet} - h_{T-outlet} \quad (13)$$

$W_T$ : Turbine specific work (J/kg)

$h_{T-inlet}$ : Specific enthalpy at turbine inlet (J/kg)

$h_{T-outlet}$ : Specific enthalpy at turbine outlet (J/kg)

The heat generated by the combustion chamber is determined by Equation (14):

$$q_{cc} = h_{CC-outlet} - h_{CC-inlet} = LCV \times \left( \frac{m_f}{m_a} \right)_{real} \quad (14)$$

$q_{cc}$ : Specific heat added in the combustion chamber (J/kg)

$h_{CC-outlet}$ : Specific enthalpy at the combustion chamber outlet (J/kg)

$h_{C-inlet}$ : Specific enthalpy at the combustion chamber inlet (J/kg)

LCV: Lower calorific value (J/kg)

The total net specific work is the difference between the turbine work and the compressor work as shown in Equation (15):

$$W_{net} = W_T - W_C \quad (15)$$

The efficiency of the cycle is calculated by:

$$\eta = \frac{W_{net}}{q_{cc}} \quad (16)$$

The methodology conducted in the thermodynamic analysis is illustrated in the chart in Figure 8. The input parameters are: the ambient pressure ( $P_{amb} = 1013$  bar), the ambient temperature ( $T_{amb} = 25$  °C), the maximum pressure ( $P_{max}$ ), the number of compressor stages ( $N_c$ ), the compressor pressure ratio ( $\pi_c$ ), the number of turbine stages ( $N_t$ ), the expansion ratio ( $\pi_t$ ) and the excess of air coefficient ( $\lambda$ ).

The analysis is realized by varying the different parameters in the GT cycle and comparing the results to select the optimal configuration related to the maximum pressure. The different parameters tested are the number of compressor stages, the number of turbine stages, the maximum pressure, and the turbine inlet temperature.



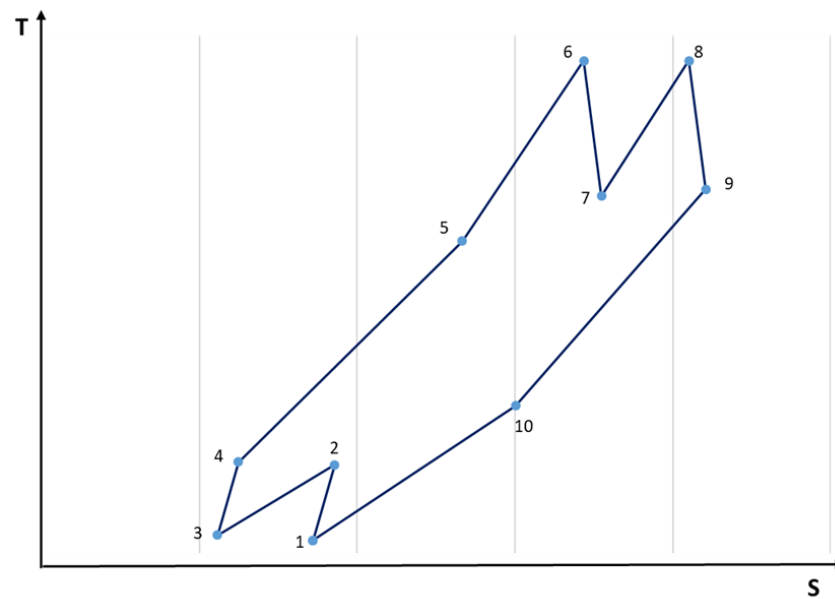


**Figure 10.** TS diagram for uncooled IRReGT. (Numbers 1-10 describe the flow passage at different stage of the cycle).

Only the HP turbine is cooled, the LP turbine is not cooled and the temperature at its inlet is limited to the material properties. In the cooled HP turbine, there is no expansion for the coolant. The expansion occurs only for the remainder mainstream. Depending on the chosen TIT at the HP turbine and on the material constraints a second combustion chamber is added. If the temperature at the outlet of the HP turbine is less than the turbine wall temperature ( $T_w$ ), the two fluids mix and expand in the LP turbine after being heated in the second combustion chamber. If there is no need for the second combustion, the two fluids directly mix and expand in the second turbine.

The detailed thermodynamic analysis and conditions are presented in [20]. The same methodology is applied to determine the coolant mass fraction needed to cool the turbine blade. The cooled turbine is considered a co-current flow heat exchanger, as illustrated in Figure 11. In the following analysis, we assume that  $T_w$  is constant and that hot gas from the mainstream flows on one side while coolant flows on the other.

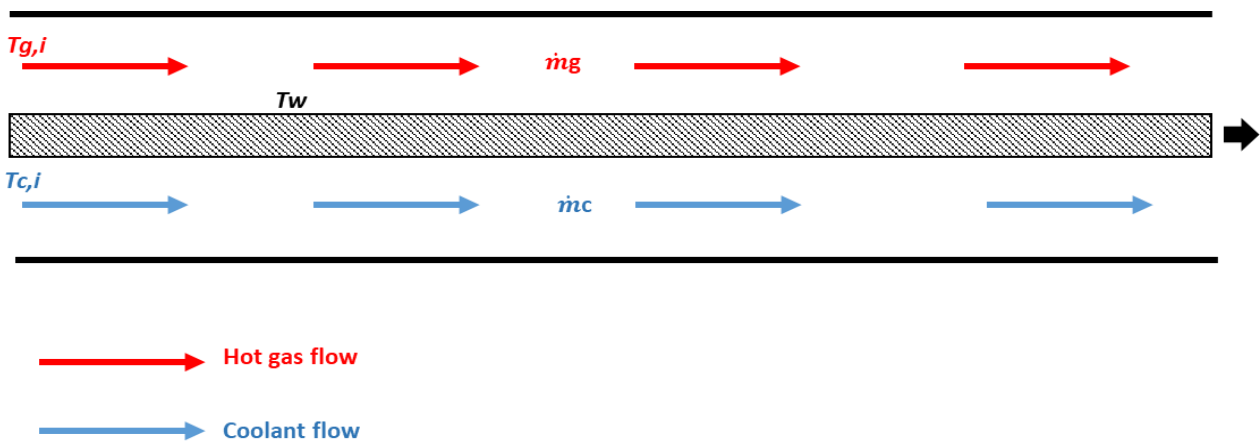


**Figure 11.** Schematic presentation of the HP cooled turbine as a heat exchanger.

This analysis aims to examine the impact of further increase of the TIT of the HP and the possibility of removing the CC2 in a way to suggest a new configuration of the range extender for SHEV.

The fraction of compressed air for turbine blade cooling is determined by:

$$X = \frac{\dot{m}_c}{\dot{m}_c + \dot{m}_g} \quad (17)$$

$X$ : Mass fraction ratio

$\dot{m}_c$ : Coolant mass flow (kg/s)

$\dot{m}_g$ : Hot gas mass flow (kg/s)

The isentropic efficiency of an uncooled turbine is determined by the ratio of the actual work to the ideal work as depicted in Figure 12a.

$$\eta_u = \frac{h_4 - h_5}{h_4 - h_{5s}} \quad (18)$$

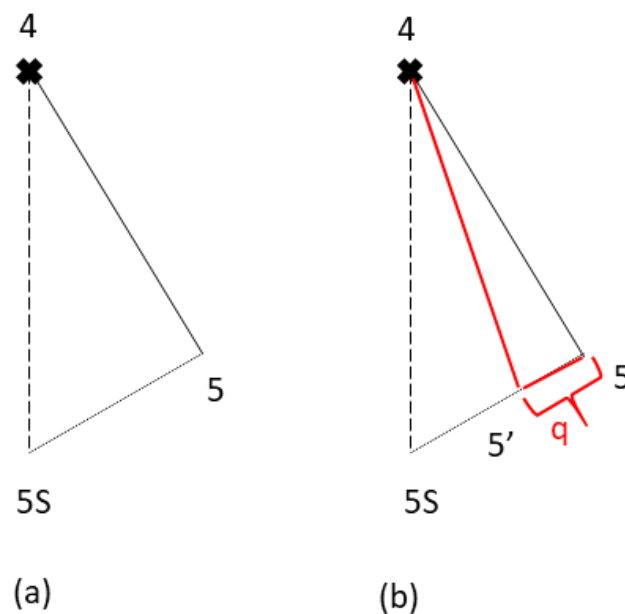


Figure 12. (a) Uncooled expansion; (b) cooled turbine.

$h_4$ : Specific enthalpy at the inlet of the turbine (kJ/kg)

$h_5$ : Specific enthalpy at the outlet of the turbine (kJ/kg)

$h_{5s}$ : Specific isentropic enthalpy at the outlet of the turbine (kJ/kg)

In a cooled turbine, the efficiency definition should take into consideration the heat extracted from the turbine blade. The decrease of the enthalpy at the outlet of the turbine is not only due to the expansion through the turbine but also due to the loss of thermal heat as illustrated in Figure 12b.

The efficiency of the cooled turbine is determined by:

$$\eta_c = \frac{h_4 - h_5 - q}{h_4 - h_{5s}} \quad (19)$$

$q$ : Heat flow that occurs between the coolant and the turbine blade (kJ/kg)

Comparing the previous two definitions, it can be concluded that the efficiency of the cooled turbine is lower than the uncooled turbine. It decreases with the increase in heat loss.

The heat flux between the hot gas and the coolant air is calculated by:

$$Q = \dot{m}_c \times C p_c \times (T_{co} - T_{ci}) = \dot{m}_g \times C p_g \times (T_{gi} - T_{go}) \quad (20)$$

$$q = X \times C p_c \times \varepsilon \times (T_w - T_{ci}) \quad (21)$$

$Q$ : Heat flow that occurs between the coolant and the turbine blade (kJ)

$C_{p_c}; C_{p_g}$ : Specific heat capacity at constant pressure (J/(kg·K))

$T_{co}$ : Coolant outlet temperature (K)

$T_{ci}$ : Coolant inlet temperature (K)

$T_{gi}$ : Gas inlet temperature (K)

$T_{go}$ : Gas outlet temperature (K)

The output net specific work is calculated using Equation (22):

$$W_{net} = [(1 - X) \times W_{HP-T} + W_{LP-T}] - [W_{LP-C} + (1 - X) \times W_{HP-C}] \quad (22)$$

$W_{HP-T}$ : HP turbine specific work (J/kg)

$W_{LP-T}$ : LP turbine specific work (J/kg)

$W_{HP-C}$ : HP turbine specific work (J/kg)

$W_{LP-C}$ : LP compressor specific work (J/kg)

Equation (23) represents the efficiency of the current cycle with a cooled HP turbine:

$$\eta = \frac{W_{net}}{(1 - X) \times q_{cc1} + q_{cc2}} \quad (23)$$

$q_{CC1}$ : Specific heat added in the first combustion chamber (J/kg)

$q_{CC2}$ : Specific heat added in the second combustion chamber (J/kg)

$q_{CC2} = 0$  if no second combustion chamber is added

### 3. Results

#### 3.1. Uncooled Cycle

The analysis is realized by varying the number of compressor stages (intercooler + compressor) for the same maximum pressure to determine the optimal configuration. Although increasing the number of compressor stages leads to a more complex system, it reduces the compressor's required work by approaching the isothermal transformation.

The results in Figure 13 show that for the same maximum pressure, the work needed by the compressor decreases with the increase of the number of stages. The addition of two compressor stages reduces the compressor work by 50 kJ/kg and increases the cycle efficiency by 4 points compared with a single stage. Adding three compressor stages reduces the compressor work by 14 kJ/kg and increases the cycle efficiency by 2 points compared with a double stage. As a result, the reduction of compressor work enhances the cycle performance by increasing the net specific work and the thermal efficiency of the gas turbine cycle.

As a result of complex issues, the dual system was chosen in this study, especially since adding further compressor stages failed to significantly improve the gas turbine cycle.

According to Figure 14, increasing the number of turbine stages improves the turbine work, as well as the net specific work. The work and the efficiency of a dual-stage turbine are higher by 65 kJ/kg and 4 points, respectively, compared with a single-stage turbine. Additional turbine stages with reheating result in an increase of less than 30 kJ/kg in turbine work and 2 points increase in the cycle thermal efficiency. Triple turbine stages did not lead to further advantages compared to the dual stages. Therefore, two expansion stages were selected.

Considering a recuperated gas turbine cycle with two compression stages and two turbine stages, a variation of the maximum pressure of the system was conducted to identify the optimal pressure in terms of higher thermal efficiency and higher specific work. The TIT was limited to 950 °C. Figure 15 illustrates the impact of increasing the pressure on the different components of the cycle.

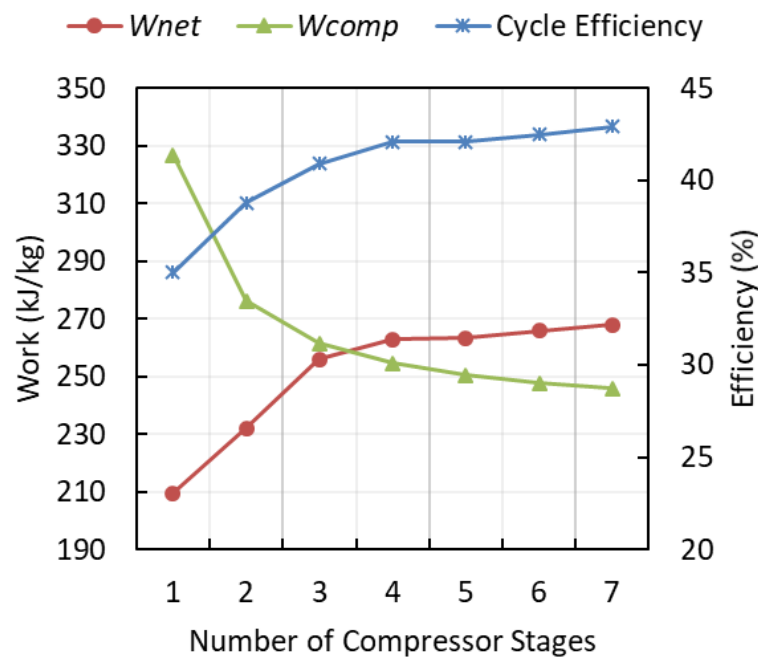


**Figure 13.** Variation of the compressor work, the net specific work, and the cycle efficiency with the number of compressor stages.

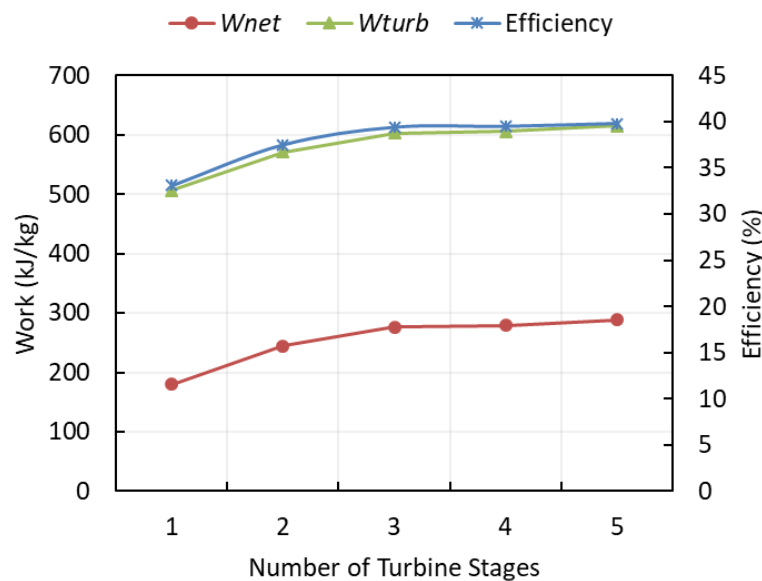


**Figure 14.** Variation of the turbine work, the net specific work, and the cycle efficiency with the number of turbine stages.

The thermal efficiency curve represents a Pareto front. It can be seen that the thermal efficiency of the gas turbine cycle increases at lower compression ratios, then when the maximum pressure reaches 9 bar a decrease in the thermal efficiency is obtained. The reason for this can be seen in the increase in the power needed to operate the compressor, which reduces the net useful power that the gas turbine can generate.

Increasing the maximum pressure leads to higher turbine work and higher net specific work. As a result, for a fixed power, less air is required in the cycle. Figure 16 shows that by increasing the maximum pressure from 4 bar to 9 bar the mass flow rate is decreased from 336 kg/s to 244 kg/s.

The benefits of increasing the turbine inlet temperature are depicted in Figure 17. The turbine specific work, as well as the cycle efficiency, are higher. However, the material

melting point limits the temperature at the inlet of the turbine. As long as the temperature does not exceed 950 °C, it is not necessary to use special materials, and the turbine can be made using familiar, low-cost alloys. Up to 1100 °C, special materials are essential. Lastly, for temperatures exceeding 1250 °C, high-cost materials are required [19].

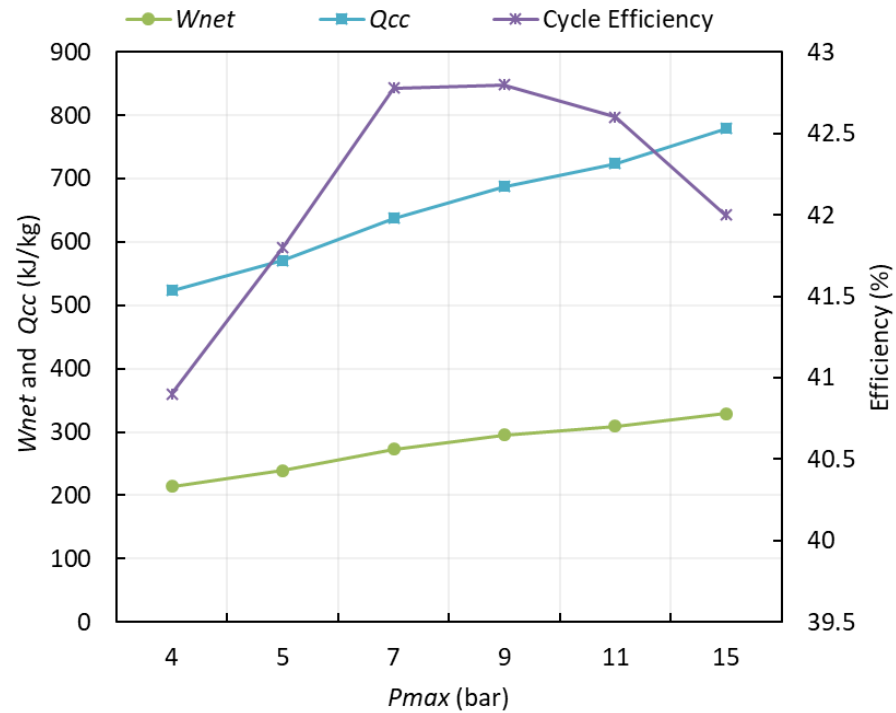


Figure 15. Variation of different parameters with the maximum pressure.

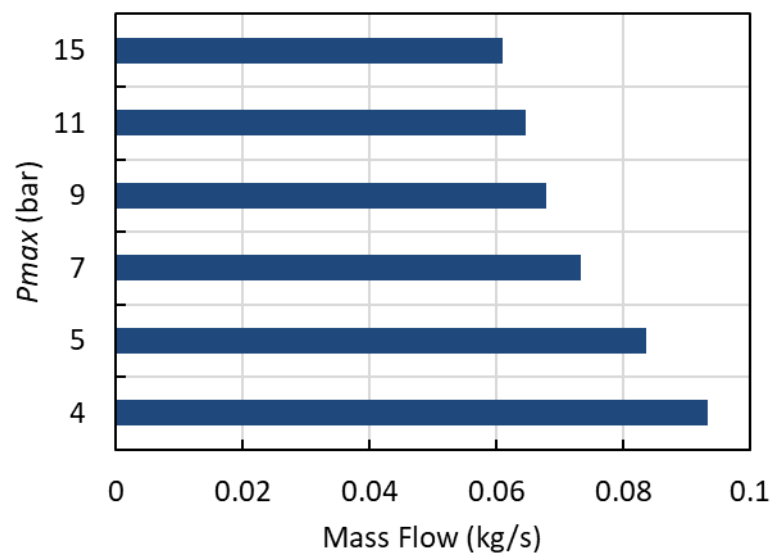


Figure 16. Variation of air mass flow rate with the maximum pressure.

### 3.2. Cooled Cycle

To increase the turbine inlet temperature, the turbine blade cooling technique is applied. Three scenarios were tested. The first scenario consists of a turbine with  $T_w = 950$  °C, which allows use of a low-cost material; the second scenario consists of  $T_w = 1100$  °C as in [20], and the last scenario is for  $T_w = 1250$  °C.

As seen in Figure 18, the cycle efficiency as well as the TIT increases with the increase of the  $T_w$ . Considering the first scenario, for  $T_w = 950$  °C, if the TIT of the HP turbine

reaches 1300 °C, there is no need for a second combustion chamber. The temperature at the outlet of the HP is 950 °C. The coolant and the mainstream mix and expand in the LP turbine. The cycle efficiency is 48.54% and the coolant mass fraction is 1.66%. The efficiency is increased by 2 points compared with the uncooled IRReGT cycle.

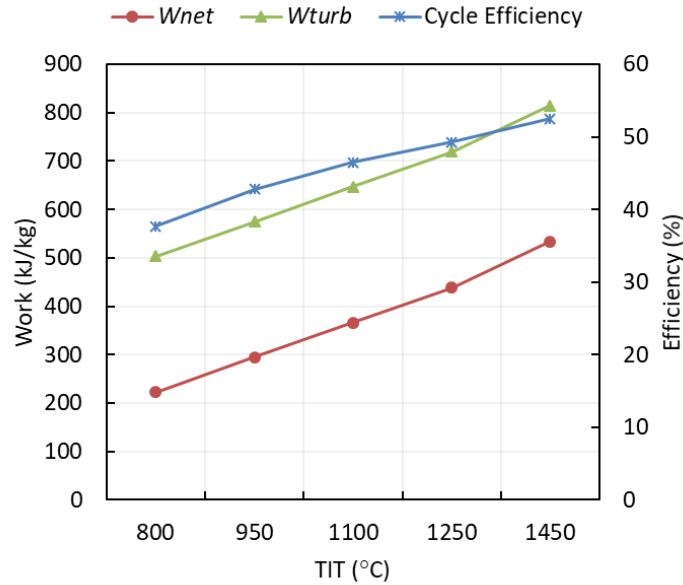


Figure 17. Variation of different parameters with the TIT.

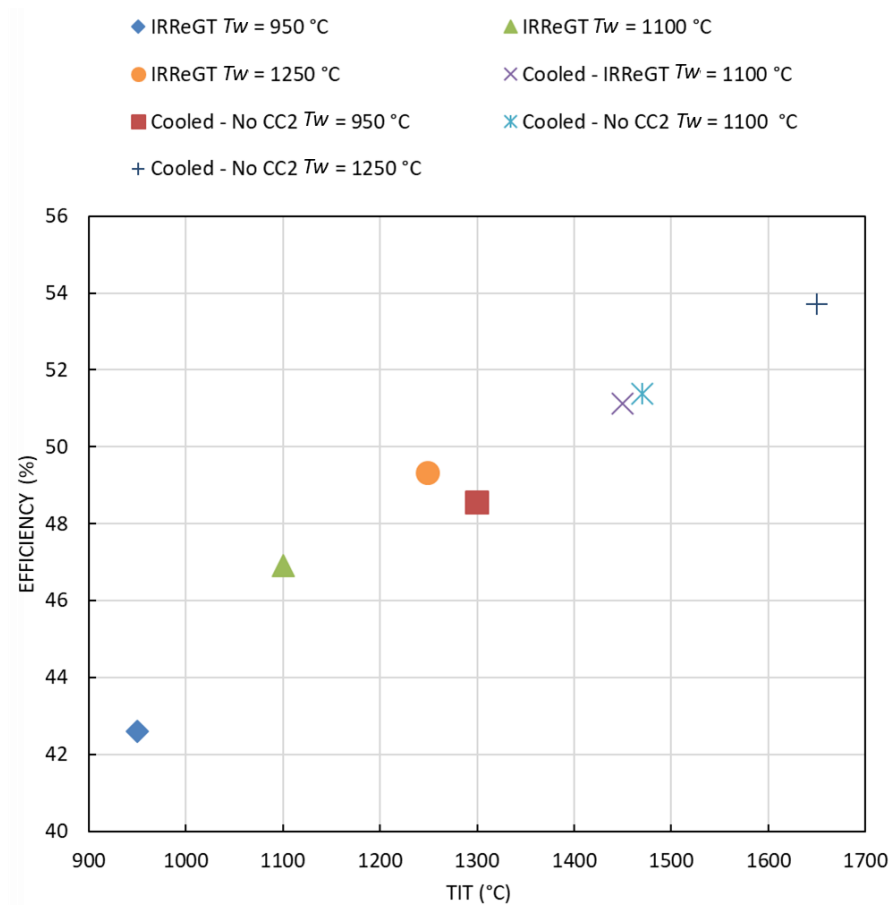


Figure 18. Variation of the GT cycle efficiency with different scenarios.



A higher efficiency of 46.9% is obtained when using more advanced materials capable of handling temperatures up to 1100 °C. When applying the cooling technique suggested by [20], the efficiency is increased by 4 points for a TIT of 1450 °C. If the TIT is increased by 20 °C, there is no need for a second combustion chamber, and the cycle efficiency is 51.5%. Hence, no significant change in the cycle efficiency but an increase in the mass flow ratio from 1.4% to 1.5%.

The last scenario describes the case of high-cost materials for which the melting temperatures are up to 1250 °C. The efficiency of the uncooled IRReGT cycle reaches 49.3%. If the TIT is further increased to 1650 °C, there is no need for another reheating and the cycle efficiency is 53.7% with a coolant mass fraction ratio of 1.4%.

#### 4. Discussion

This paper intends to determine a suitable GT cycle to extend the autonomy of an electric car. The configuration consists of a generator that transforms the mechanical power from the GT cycle into electricity to charge the battery of the vehicle.

At first, it is necessary to determine the properties of the cycle and the suitable operating conditions that result in an increase the cycle efficiency.

Several conclusions can be drawn from the findings outlined in the previous sections.

Using multistage compressions and multistage expansions leads to an increase in cycle efficiency. It will, therefore, result in a more complex, more expensive, and heavier GT cycle. Due to this, a dual stage compression with an intercooler and a dual stage expansion with reheating are selected. In this way, the GT cycle will operate with high efficiency and be sufficiently compact to be integrated into the EV.

A Pareto front is obtained when the maximum pressure of the GT cycle is varied. Cycle efficiency increases for pressures under 9 bar, then decreases for pressures above 9 bar. Because of this, 9 bar is chosen as the maximum pressure.

The increase of the GT cycle temperature has numerous benefits on the cycle efficiency but due to turbine material constraints and cost, only limited temperature increases are possible.

The advantage of applying the blade cooling technique is the ability to increase the TIT with no limitations due the material melting temperatures or constraints. This results in increasing the overall cycle efficiency.

Different scenarios are considered depending on the material chosen for the turbine. As the turbine material can handle higher temperatures, the cycle efficiency increases, as well as the cost. As a result, a  $T_w$  of 1100 °C is considered optimal.

By comparing the results of different configurations we can conclude that if we further increase the TIT of the HP turbine, there is no need for CC2 with no significant variation in the GT cycle efficiency. As a result, the system becomes more compact, less complex, and less expensive.

Despite the advantages of cooling blades, the technique has some drawbacks as well. When the cooling technique is applied, the turbine efficiency is reduced. In addition, after the expansion in the HP turbine, when mixing occurs between the mainstream and the coolant, a turbine work is lost due to the mixture's lower temperature. Furthermore, applying the blade cooling technique leads to higher costs and more complexity in the system.

#### 5. Conclusions

This study aims to select a new powertrain to replace the internal combustion engine due to climate change. The optimal cycle configuration in terms of higher efficiency is selected based on a sensibility analysis and a thermodynamic study using VBA and Refprop.

The intercooled recuperated gas turbine cycle with a cooled HP turbine and an uncooled LP turbine is the most optimal among the several GT options assessed, given its high efficiency, and lower complexity.

The HP turbine is cooled by pressurized air extracted from the first compressor and the LP turbine is uncooled. Using previous configurations, it is possible to eliminate the second combustion by increasing the TIT of the HP turbine. Therefore, both the weight and the price of the overall system can be reduced without significantly affecting the efficiency cycle and the coolant mass fraction. For a maximum pressure of 9 bar and a TIT of the HP turbine of 1470 °C, the cycle reaches higher efficiency (51.39%) than the standard IRReGT cycle (46.9%), and approximately the same efficiency as the IRReGT cycle with a cooled HP turbine.

In future work, the authors will further elaborate on a detailed study of the cost and weight of the overall system. In addition, the authors will evaluate the impact of increased temperature on NO<sub>x</sub> emissions.

**Author Contributions:** J.N. carried out the modeling and simulation, and the analysis under the support and supervision of M.N. and C.B. All authors have read and agreed to the published version of the manuscript.

**Funding:** This research received no external funding.

**Data Availability Statement:** Not applicable.

**Conflicts of Interest:** The authors declare no conflict of interest.

## Abbreviations

amb	ambient
CC	Combustion Chamber
CH <sub>4</sub>	Methane
CO <sub>2</sub>	Carbon dioxide
$C_p$	Specific heat capacity at constant pressure (J/(kg·K))
EV	Electric Vehicle
GT	Gas turbine
GTs	Gas turbines
$h$	Specific enthalpy (J/kg)
H <sub>2</sub> O	Water
HEX	Heat exchanger
HP	Hot Pressure
ICE	Internal combustion engine
IRReGT	Intercooled recuperated reheated gas turbine cycle
LP	Low pressure
$m_a$	Mass of air
$m_f$	Mass of fuel
$m_t$	Total mass
N <sub>2</sub>	Nitrogen
N <sub>c</sub>	Number of compressor stages
N <sub>t</sub>	Number of turbine stages
O <sub>2</sub>	Oxygen
$q$	Heat transfer (J/kg)
$Q$	Heat transfer (J)
$r$	Excess of air
SHEV	Series hybrid electric vehicles
$T$	Temperature (K)
TIT	Turbine inlet temperature (K)

## Subscripts

1	First
2	Second
4	Turbine inlet value
5	Turbine outlet value without cooling

$5s$	Turbine outlet isentropic value
$5'$	Turbine outlet value with cooling
$c$	coolant
$i$	Inlet
$g$	Mainstream gas
$o$	outlet
$w$	wall
<b>Greek Symbols</b>	
$\eta$	Efficiency of the GT cycle
$\eta_u$	Efficiency of the uncooled turbine
$\eta_c$	Efficiency of the cooled turbine
$\pi_c$	Compression ratio
$\pi_t$	Expansion ratio
$\lambda$	Excess of air ratio
$\chi$	Extracted mass fraction ratio
$\epsilon$	Effectiveness of the turbine as a heat exchanger

## References

- Climate Action—European Commission. Transport Emissions. Available online: [https://ec.europa.eu/clima/policies/transport\\_en](https://ec.europa.eu/clima/policies/transport_en) (accessed on 8 September 2021).
- Ji, F.; Zhang, X.; Du, F.; Ding, S.; Zhao, Y.; Xu, Z.; Wang, Y.; Zhou, Y. Experimental and Numerical Investigation on Micro Gas Turbine as a Range Extender for Electric Vehicle. *Appl. Therm. Eng.* **2020**, *173*, 115236. [[CrossRef](#)]
- Christodoulou, F.; Giannakakis, P.; Kalfas, A.I. Performance Benefits of a Portable Hybrid Micro-Gas Turbine Power System for Automotive Applications. *J. Eng. Gas Turbines Power* **2011**, *133*, 022301. [[CrossRef](#)]
- Chrysler Corporation. *History of Chrysler Corporation Gas Turbine Vehicles*; Chrysler Corporation: Auburn Mills, MI, USA, 1979.
- Corporation, B. *Popular Science*; Bonnier Corporation: Winter Park, FL, USA, 1974.
- Norbye, J. Turbine Drives Chevy Truck. In *Popular science*; Bonnier Corporation: Winter Park, FL, USA, 1965.
- Cunha, H.E.; Kyprianidis, K.G. Investigation of the Potential of Gas Turbines for Vehicular Applications. *Am. Soc. Mech. Eng.* **2012**, *44694*, 51–64. [[CrossRef](#)]
- Karvountzis-Kontakiotis, A.; Andwari, A.M.; Pesyridis, A.; Russo, S.; Tuccillo, R.; Esfahanian, V. Application of Micro Gas Turbine in Range-Extended Electric Vehicles. *Energy* **2018**, *147*, 351–361. [[CrossRef](#)]
- Nader, W.B. Methodology for the Selection and Optimization of Energy Converters for Automotive Powertrain Applications. Ph.D. Thesis, PSL Université, Paris, France, 2019.
- Sherwin, K. *Introduction to Thermodynamics*; Springer Science & Business Media: Berlin/Heidelberg, Germany, 2012.
- Giampaolo, T. *Gas Turbine Handbook: Principles and Practice*; The Fairmont Press, Inc.: Lilburn, GA, USA, 2009.
- Saravanamuttoo, H.I.H.; Rogers, G.F.C.; Cohen, H. *Gas Turbine Theory*; Pearson Education: London, UK, 2009.
- Nowak, G.; Wróblewski, W.; Nowak, I. Convective cooling optimization of a blade for a supercritical steam turbine. *Int. J. Heat Mass Transf.* **2012**, *55*, 4511–4520. [[CrossRef](#)]
- Wu, W.; Yao, R.; Wang, J.; Su, H.; Wu, X. Leading edge impingement cooling analysis with separators of a real gas turbine blade. *Appl. Therm. Eng.* **2022**, *208*, 118275. [[CrossRef](#)]
- Liang, C.; Rao, Y.; Luo, J.; Luo, X. Experimental and Numerical Study of Turbulent Flow and Heat Transfer in a Wedge-shaped Channel with Guiding Pin Fins for Turbine Blade Trailing Edge Cooling. *Int. J. Heat Mass Transf.* **2021**, *178*, 121590. [[CrossRef](#)]
- Yerane, K.; Rao, Y. A review of recent studies on rotating internal cooling for gas turbine blades. *Chin. J. Aeronaut.* **2021**, *34*, 85–113. [[CrossRef](#)]
- Mackay, R. *Development of a 24 kW Gas Turbine-Driven Generator Set for Hybrid Vehicles*; SAE Technical Paper 940510; SAE International: Warrendale, PA, USA, 1994. [[CrossRef](#)]
- Nader, W.S.B.; Mansour, C.J.; Nemer, M.G. Optimization of a Brayton external combustion gas-turbine system for extended range electric vehicles. *Energy* **2018**, *150*, 745–758. [[CrossRef](#)]
- Barakat, A.A.; Diab, J.H.; Badawi, N.S.; Nader, W.S.B.; Mansour, C.J. Combined cycle gas turbine system optimization for extended range electric vehicles. *Energy Convers. Manag.* **2020**, *226*, 113538. [[CrossRef](#)]
- Najib, J.; Nemer, M.; Bouallou, C. Thermodynamic Study of a Cooled Micro Gas Turbine for a Range Extended Electric Vehicle. *Chem. Eng. Trans.* **2021**, *88*, 1255–1260.
- Al Khoury, J.; Nader, W.B. Design and simulation of turbogenerators for series hybrid electric vehicles. *Energy Convers. Manag.* **2021**, *236*, 114078. [[CrossRef](#)]